PCCP

Accepted Manuscript

ROYAL SOCIETY OF CHEMISTRY

www.rsc.org/pccp

Physical Chemistry Chemical Physics
CREATED USING THE RSC LaTeX PCCP ARTICLE TEMPLATE – SEE www.rsc.org/electronicfiles FOR DETAILS
ARTICLE TYPE
www. rsc.org/xxxxxx | XXXXXXXX

Activity of ZnO polar surfaces: An insight from surface energies†

Chunguang Tang,*[a] Michelle J. S. Spencer,[a,b]‡ and Amanda S. Barnard[a]

Received Xth XXXXXXXXXX 20XX, Accepted Xth XXXXXXXXX 20XX
First published on the web Xth XXXXXXXXXX 200X
DOI: 10.1039/b000000x

The calculation of the accurate surface energies for (0001) surfaces of wurtzite ZnO is difficult because it is impossible to decouple the two inequivalent (0001)-Zn and (000$\bar{1}$)-O surfaces. By using a heterojunction model we have transformed the uncertainty of the surface energies into that of interface energies which is much smaller than the former and hence estimated the surface energies to a high degree of accuracy. It is found that oxygen terminated (000$\bar{1}$)-O face of wurtzite phase and ($\bar{1}\bar{1}\bar{1}$)-O of zinc blende phase are more stable than their Zn-terminated counterparts within the major temperature and oxygen partial pressure range accessible to experiment. The instability of Zn-terminated polar surfaces explains the experimentally observed high activity of these surfaces. The effects of native surface vacancies on the surface energies have also been discussed. These results shed insights on the modification of surface stability and activity of ZnO nanoparticles.

1 Introduction

As a material with a wide range of applications in optoelectronic and electronic devices, catalysis, and gas sensing, zinc oxide (ZnO) has seen extensive research interests recently. Under ambient conditions, macroscopically ZnO is in its hexagonal wurtzite (WZ) phase, and its cubic zinc blende (ZB) phase is metastable, although the atomic structures of these two phases differ only at the third atomic neighbor. At nanoscale where many applications of ZnO occur, its performance and properties depends on its surfaces owing to the high surface to volume ratio. For WZ ZnO, mainly four low-index surfaces are of interest: the nonpolar (10$\bar{1}$0) and (11$\bar{2}$0), and the polar zinc-terminated (0001)-Zn and oxygen-terminated (000$\bar{1}$)-O.

Compared with the nonpolar surfaces, the polar surfaces are more intriguing from both scientific and technological points of view. Scientifically, the stabilization mechanism of such unstable polar surfaces has attracted extensive attention.[1–4] Technologically, the polar ZnO surfaces have been reported to be the active ones for gas molecule adsorptions and surface reactions.[5] For the polar surfaces, the Zn-terminated ones are found to be more active than the O-terminated ones. For example, the growth of hexagonal rods in plasma deposition is found to be along the [0001] direction of Zn polarity, with pyramidal islands nucleating and growing on the polar (0001) faces,[6] and in the growth of nanocantilever arrays the (0001) face is found chemically more active than the (000$\bar{1}$) face.[7] Such higher activity is also found in the four Zn-terminated surfaces of the octahedral ZB core of tetrapod ZnO nanoparticles.[8,9] On the theoretical side, a phase-field simulation of ZnO film growth suggested easier nucleation on Zn-terminated surfaces.[10]

A reasonable hypothesis for explaining the higher activity of Zn-terminated surfaces is that the Zn-terminated surfaces have higher surface energies than their O-terminated counterparts do. Experimental confirmation of this hypothesis is difficult as the measured surface energies are average values for all exposed surfaces.[11]

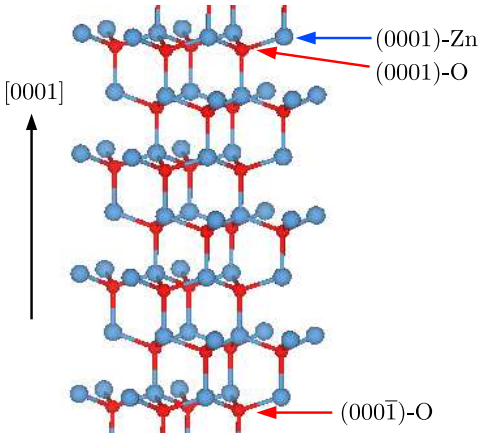

Fig. 1 A (0001) ZnO slab. If the top (0001)-Zn layer is removed, the top (0001)-O layer has three dangling bonds for each surface atom and hence is inequivalent to the bottom (000$\bar{1}$)-O layer, of which each O atom has one dangling bond. Red: O, blue: Zn.

Here we support the above hypothesis about the polar sur-

† Electronic Supplementary Information (ESI) available: [details of any supplementary information available should be included here]. See DOI: 10.1039/b000000x/

[a] *Virtual Nanoscience Laboratory, CSIRO, Australia*
[b] *School of Applied Sciences, RMIT University, Melbourne VIC 3001, Australia*

face activity by estimating the surface energies of (0001)-Zn and $(000\bar{1})$-O faces based on the wedge and heterojunction methods. Our results show that, in oxygen-rich atmosphere which corresponds to most experiment conditions, (0001)-Zn has higher surface energy and is more active than $(000\bar{1})$-O.

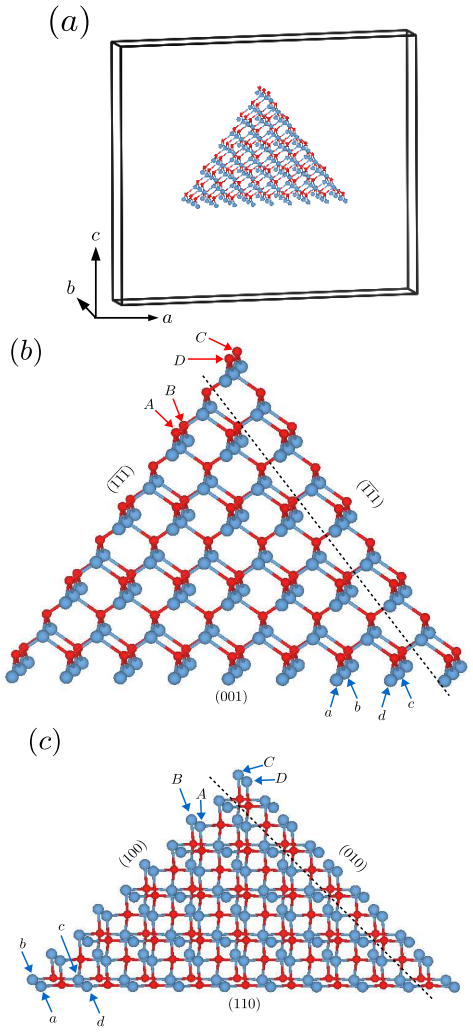

Fig. 2 The prisms used for calculating energies of polar surfaces of ZB ZnO. (a) A supercell structure showing the prism and the vacuum. The prism is periodic along ***b*** direction and separated from its images along ***a*** and ***c*** directions. (b) For $(\bar{1}\bar{1}\bar{1})$-O which uses (100)-Zn as input; (c) For (100)-Zn which uses nonpolar (110) as input. The dashed line indicates some atoms are cut off to change prism size. Zn: blue, O: red.

2 Methods

Our method is slightly different from the wedge and heterojunction approaches where the surface atoms were passivated by pseudohydrogen atoms and the atoms in the system were allowed to relax. Instead we use unpassivated surfaces, with dipole correction applied and all the atoms fixed at their ideal bulk position. The energy thus obtained is the truncated surface energy, and the relaxed surface energies are later obtained by considering the relaxation contribution of the corresponding surface using the standard slab geometry, with the other surface fixed. The total energy calculations are performed using the VASP code [12] with the projector-augmented-wave pseudopotential as supplied in VASP, the GGA-PBE exchange-correlation functional, and a plane wave basis with an energy cutoff of 500 eV. A Monkhorst-Pack k-point sampling mesh of $6 \times 6 \times 4$ was used for the hexagonal unit cell, and the number of k-point was reduced for larger cells. In the directions which involves vacuum only one k-point was used. As shown in Table 1, the bulk structure parameters optimized under these settings are in good agreement with their experimental values.

Table 1 Calculated and experimental lattice parameters for WZ ZnO.

Source	a (Å)	c (Å)	c/a	u
This work	3.2862	5.3005	1.6130	0.3793
Expt. (Ref. [13])	3.2496	5.2042	1.6018	0.3819
Expt. (Ref. [14])	3.2501	5.2071	1.6021	0.3817

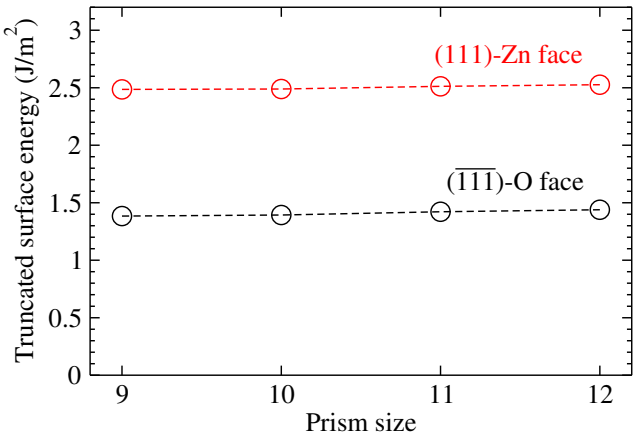

Fig. 3 Truncated surface energies of (111) face versus the size of prisms used.

The truncated surface energy of $(\bar{1}\bar{1}\bar{1})$-O face can be calculated using the triangle prism of ZnO shown in Fig. 2(a), which contains a (001)-Zn face and two equivalent $\{\bar{1}\bar{1}\bar{1}\}$-O faces, and that of (111)-Zn can be obtained by swapping Zn and O atoms. The prism is periodic along the intersection of the faces (i.e., along AB) and separated from its periodic images in other directions by vacuum of more than 10 Å. When

one layer of ZnO is removed, as indicated by the dashed line, the energy difference between the old and new prisms can be expressed as [15]

$$\begin{aligned}\Delta E = \quad & \Delta \quad n_{\mathrm{Zn}}\mu_{\mathrm{Zn}} + \Delta n_{\mathrm{O}}\mu_{\mathrm{O}} + \Delta s_{(\overline{1}\overline{1}\overline{1})}\gamma^{0}_{(\overline{1}\overline{1}\overline{1})} \\ & + \quad \Delta s_{(100)}\gamma^{0}_{(100)} \end{aligned} \tag{1}$$

where n and μ are the number of atoms in the prisms and their chemical potential, respectively, and Δs and γ^0 are the change in surface area and the truncated surface energy, respectively. In the case shown in Fig. 2(a), Δn_{Zn}=Δn_{O}=-9 (note atom D is the periodic image of atom C), and $\Delta s_{(\overline{1}\overline{1}\overline{1})}$ and $\Delta s_{(001)}$ equal the rectangles $ABCD$ and $abcd$, respectively. The energy $\gamma^0_{(\overline{1}\overline{1}\overline{1})}$ can be calculated from Eq. (1) once $\gamma^0_{(100)}$ is obtained similarly using the configuration in Fig. 2(b), where face (110) is nonpolar and its truncated surface energy is calculated using the standard slab approach. Note that in Fig. 2(b) Δn_{Zn} and Δn_{O} are not equal and thus the calculated $\gamma^0_{(100)}$ and hence $\gamma^0_{(\overline{1}\overline{1}\overline{1})}$ explicitly depends on μ_{O}. The chemical potentials μ_{Zn} and μ_{O} in ZnO can vary in a range constrained by the facts that Zn and O are in equilibrium with bulk ZnO and that bulk ZnO is stable against decomposition into bulk Zn and oxygen gas. Explicitly, one has $\mu_{\mathrm{Zn}} + \mu_{\mathrm{O}} = E_{\mathrm{ZnO}}$, $\Delta H_{\mathrm{ZnO}} \leq \Delta\mu_{\mathrm{O}} = \mu_{\mathrm{O}} - 0.5E_{\mathrm{O_2}} \leq 0$ and $\Delta H_{\mathrm{ZnO}} \leq \Delta\mu_{\mathrm{Zn}} = \mu_{\mathrm{Zn}} - E^{\mathrm{bulk}}_{\mathrm{Zn}} \leq 0$, where E is the calculated total energy at 0 K, and the formation enthalphy $\Delta H_{\mathrm{ZnO}} = E_{\mathrm{ZnO}} - 0.5E_{\mathrm{O_2}} - E^{\mathrm{bulk}}_{\mathrm{Zn}}$ is calculated to be -2.89 eV, compared with previously calculated value [16] of -2.84 eV and experimental value [17] -3.50 eV. The oxygen in ZnO is assumed to be in equilibrium with the ambient atmosphere, and hence $\mu_{\mathrm{O}} = 0.5\mu_{\mathrm{O_2}}$ is a function of temperature and pressure.

3 Results and discussion

We calculated γ^0 of (111) face with respect to prism size N, defined by the number of ZnO in the base (100) face in Fig. 2(a), ranging from 9 to 12, and the values are plotted in Fig. 3 for the oxygen rich limit, or μ_{O}=-4.93 eV, half the DFT energy of an O_2 molecule. As can be seen, the truncated surface energy has been converged within 0.1 J/m^2. For N=12, we obtained γ^0 of 1.44 and 2.53 J/m^2 for $(\overline{1}\overline{1}\overline{1})$-O and (111)-Zn, respectively, of which the sum is close to 4.05 J/m^2, the truncated cleavage energy of the two coupled surfaces based on a slab geometry of 12 Zn-O double layers. The values at N=12 are used for the following calculations of (0001) surface energies.

With γ^0 of (111) faces known, γ^0 of (0001) faces can be estimated using the interface models shown in Fig. 4(a). The ZB/ZB model is just a ZB slab as the reference, and in the WZ/ZB heterojunction the WZ phase is stretched along the interface plane to the size of ZB. The energy difference between the two models, for the case in Fig. 4(a), can then be written as [18]

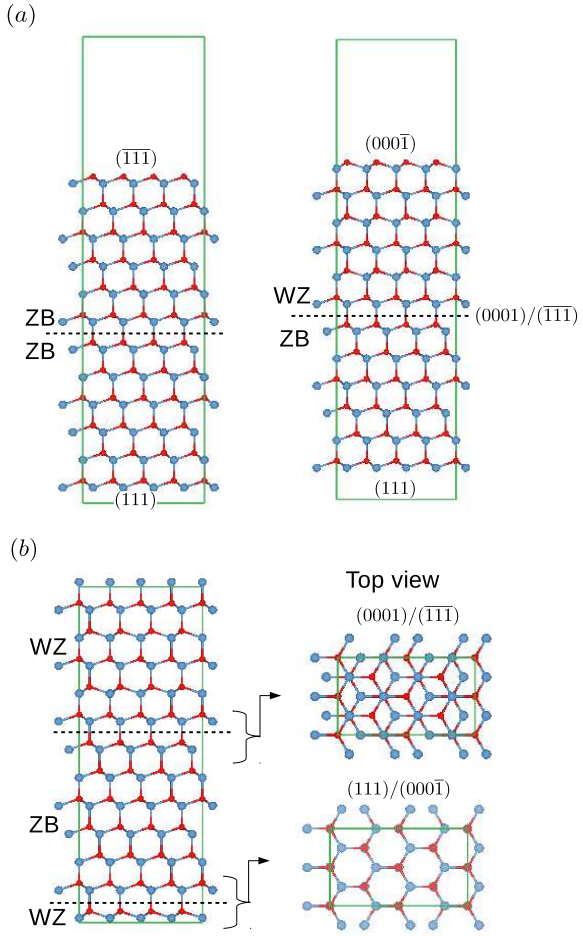

Fig. 4 (a) Interface models used for (0001) surface energy calculation. The lattice of WZ phase was stretched to that of ZB phase along the interface plane. (b) The vacuum-free WZ/ZB interface model for estimating the interface energy range. The two interfaces are inequivalent: the (0001)/($\overline{1}\overline{1}\overline{1}$) interface is staggered and the (111)/(000$\overline{1}$) interface is eclipsed. Zn: blue, O: red.

$$\begin{aligned}\Delta E = \quad & S \quad (\gamma^0_{(000\overline{1})} - \gamma^0_{(\overline{1}\overline{1}\overline{1})}) + p(e_{\mathrm{WZ}} - e_{\mathrm{ZB}}) \\ & + \quad pE_{\mathrm{s}} + SE_{\mathrm{i}} \end{aligned} \tag{2}$$

where S is the interface area, p is the number of ZnO unit in the top half of the slab, e is energy per ZnO unit in unstrained bulk WZ or ZB phase, E_{s} is the strain energy per ZnO unit resulted from the stretch of bulk WZ corresponding to the top half of the slab, and E_{i} is the formation energy of the interface, which is between (0001)-Zn and $(\overline{1}\overline{1}\overline{1})$-O for the case in Fig. 4(a). The values for $e_{\mathrm{WZ}} - e_{\mathrm{ZB}}$ and E_{s} are found from bulk phase calculations to be -0.012 eV/ZnO and 0.40 meV/ZnO,

respectively. If E_i could be calculated independently, then the energy of surface $(000\bar{1})$-O could be calculated unambiguously. Obviously, one can not use the WZ/ZB slab in Fig. 4(a) to calculate the interface energy because the surface energy is unknown. If one builds a vacuum-free heterojunction model, as shown in Fig. 4(b), then the two interfaces included in this model are not identical. At one interface the ethane-like O_3Zn-OZn_3 conformation is staggered and at the other it is eclipsed (see Fig. 4(b)). Since these two interfaces are coupled in a way similar to the case of (0001) polar surfaces, their energies can not be unambiguously defined.

Nevertheless, we can use the vacuum-free heterojunction model to estimate the range of E_i. By substracting the corresponding WZ and ZB bulk energies from that of the vacuum-free heterojunction we calculated the energy sum of the two coupled interfaces to be 12.6 mJ/m^2, which defines the upper limit of the energy for each interface. The lower limit of the interface energy is zero. With these numbers as input, the resulting γ^0 ranges for (0001)-Zn and $(000\bar{1})$-O surfaces, at O-rich limit, are calculated to be 2.49±0.0063 and 1.35±0.0063 J/m^2, respectively, summing to 3.84 J/m^2, as opposed to the 3.80 J/m^2, the truncated cleavage energy of (0001)-coupled faces based on a slab geometry of 14 Zn-O double layers.

The above method of estimating the uncertainty of (0001) surface energies, in principle, can be applied to any other polar surfaces as long as one can establish proper interface models. Because at the interfaces the dangling bonds are somewhat passivated, the energy cost for creating a vacuum-free heterojunction is usually smaller than that for two coupled polar surfaces. In other words, the uncertainty of interface energies would in general be smaller than that of surface energies, which means we can get an improved estimate of surface energies. The extent of improvement, of course, depends on the extent of local structure distortion at the interface. In the case studied here, the local structure at the WZ/ZB interfaces is very close to the bulk structure and so a quite small uncertainty is obtained.

Once γ^0 is known, relaxed surface energy γ can be calculated using a slab geometry by only allowing the atoms on the side of interest to relax, with the other side fixed. The slab and the vacuum layer should be thick to assure energy convergence and negligible interaction between the two sides. We have applied this method on nonpolar slabs and the results are consistent with those for fully relaxed slabs. Using a slab of 14 double layers with 3 of them fixed on one side, we obtained the relaxation energy, equivalent to $\gamma-\gamma^0$, of (0001)-Zn and $(000\bar{1})$-O surfaces to be -0.10 and -0.39 J/m^2, respectively, in good agreement with the total relaxation energy -0.49 J/m^2 of the whole slab with only a middle Zn-O layer fixed. The ranges of γ and γ^0, at the oxygen rich limit, were summarized in Table 2, along with other reported theoretical values. A direct comparison between the results here and the experimental surface energy data is difficult as the latter are scarce and, more importantly, not for a particular surface but averaged for all exposed ones.[11] Nevertheless, the energies for (0001)-coupled surfaces reported here agree reasonably well with previous reported values.[20] We noted that the energies for (0001)-Zn and $(000\bar{1})$-O from Ref. [19] are higher than the values reported here because in Ref. [19] a slab with both surfaces terminated by the same species was used and hence, as mentioned above, the surface energies are for a mixture of two inequivalent surfaces. On average such mixed surface structures have more surface dangling bonds than those of (0001)-Zn and $(000\bar{1})$-O surfaces and hence have higher energies.

Table 2 Truncated (γ^0) and relaxed (γ) surface energies for (111) faces of ZB-ZnO and (0001) faces of WZ-ZnO at oxygen rich limit. The relaxed surface energies of Zn- and O-terminated faces are calculated using a slab geometry with one side fixed. Data from Ref. [19] correspond to $\Delta\mu_{Zn} \approx -3.0$ eV, which is interpreted as oxygen rich condition. The experiment value is an average of the existing surfaces.

Face	γ^0 (J/m^2)	γ (J/m^2)
(111)-Zn	2.53	2.46
$(\bar{1}\bar{1}\bar{1})$-O	1.44	1.02
(111)-coupled	4.05	3.55
(0001)-Zn	2.49±0.0063	2.39±0.0063
$(000\bar{1})$-O	1.35±0.0063	0.96±0.0063
(0001)-coupled	3.80	3.31
(0001)-coupled (Ref. [20])	∼3.81	∼3.4
(0001)-Zn (Ref. [19])		∼3.8
$(000\bar{1})$-O (Ref. [19])		∼1.1
Experiment (Ref. [11,21])		2.55±0.23

To illustrate the influence of temperature and oxygen pressure, we have plotted in Fig. 5 the polar surface energies as a function of oxygen chemical potential μ_O. Several features are worthy of notice. (i) The surface energies of (0001) and those of (111) are almost identical, with difference smaller than 0.1 J/m^2. This is not surprising since in both ZB and WZ phases the atoms have similar local structures and only differ at the third atomic neighbor. (ii) For both (111) and (0001) surfaces, the O-terminated surfaces decreases their energies by ∼0.4 to 0.5 J/m^2 through surface relaxation, while the Zn-terminated surface energies decrease only by ∼0.1 J/m^2. This probably results from the fact that the relaxation of the surface Zn-O double-layer at the O-terminated surface is much more substantial than at the Zn-terminated one, a phenomenon previously reported.[1,20] (iii) The surface energies changes linearly with oxygen chemical potential. At high μ_O, which corresponds to low temperature and high oxygen partial

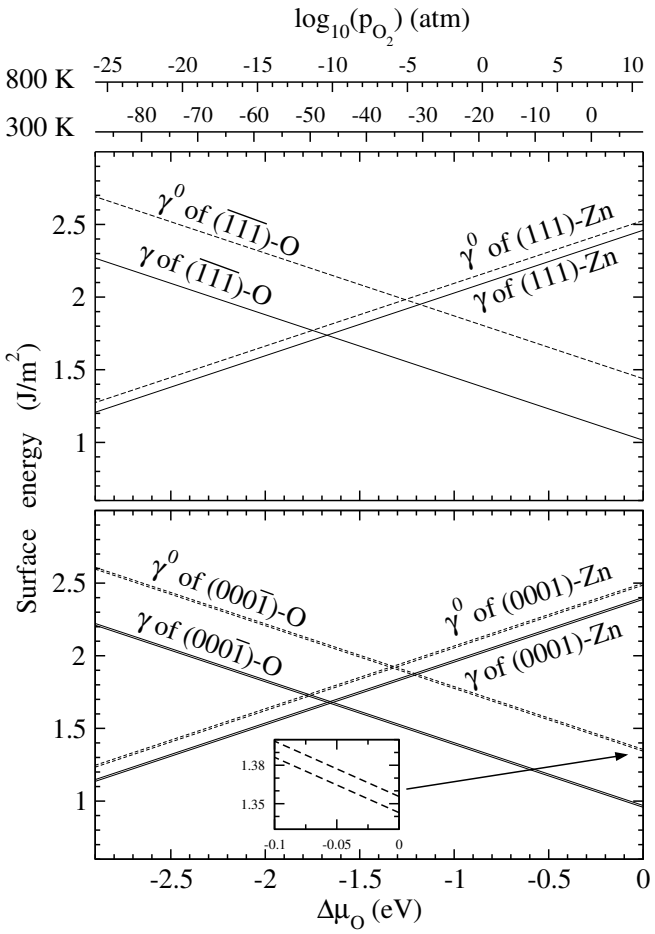

Fig. 5 Truncated (γ^0) and relaxed (γ) surface energies of (111) and (0001) faces as a function of oxygen chemical potential μ_O. For (0001) faces, the surface energies are uncertain within a very small range represented by two parallel dashed or solid lines. $\Delta\mu_O$=0 corresponds to oxygen rich limit. The pressure of O_2 corresponding to $\Delta\mu_O$ is shown for temperature at 300 K and 800 K, respectively.

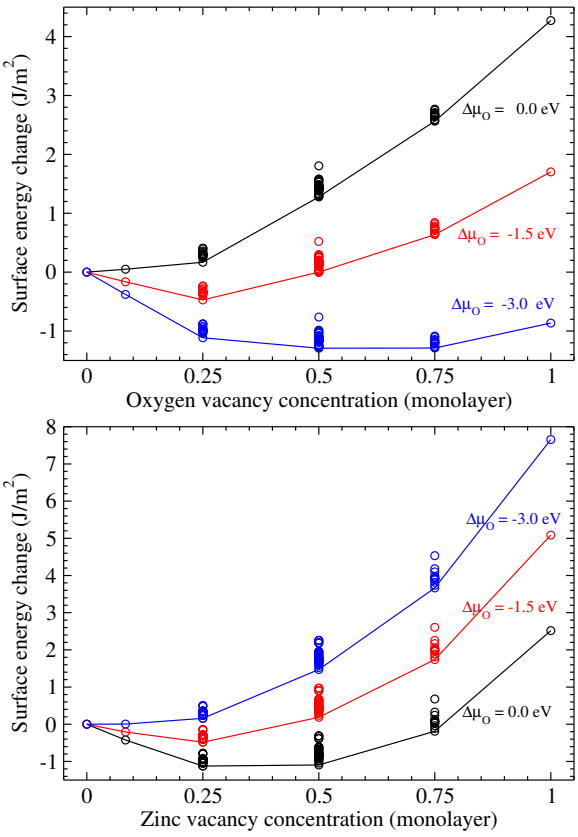

Fig. 6 The change of surface energy for (000$\bar{1}$)-O surface (top) and (0001)-Zn surface (bottom) with respect to vacancy concentration and $\Delta\mu_O$. Each circle denotes a surface configuration considered, and those with lowest energies are interlinked with solid lines.

pressure, Zn-terminated surfaces have higher energies than O-terminated ones, and as μ_O shifts towards its lower limit the Zn-terminated surfaces become more stable. The atmosphere for ZnO growth is usually somewhat oxygen rich as oxygen is a necessary component, and hence within the experimental window of temperature and pressure the Zn-terminated surfaces are usually less stable and more active than the O-terminated ones, as found in a series of experiments.[6–9]

The above results for defect-free surfaces serve as a base for studying the more complicated surfaces with defects or molecule adsorption, which, depending on the environmental conditions, can stabilize the polar surfaces. For example, for (000$\bar{1}$)-O surface honeycomb-like[22] structures, surface reconstruction and hydrogen adsorption[23] have been reported, and for (0001)-Zn surfaces islands and triangular pits[2] have been reported. Here, instead of exhaustively examing all the possible defective surface structures, we illustrate the influence of surface vacancies on the surface energies. The change of surface energy for a ZnO surface with a θ coverage of vacancies V_X (X being Zn or O) can be defined as

$$\Delta\gamma(\theta, V_X) = \frac{E(\theta, V_X) - E_0 + n_X\mu_X}{A} \qquad (3)$$

where $E(\theta, V_X)$ and E_0 are the energy of slab with and without vacancies, respectively, n_X is the number of vacancies, and A is the surface area (of one side of the slab). A rectangular (0001) slab of surface area $\sim 10\times 11$ Å^2, with 12 Zn atoms on one side and 12 O atoms on the other, was used as the reference structure.

The change of surface energy with respect to surface vacancy concentration and $\Delta\mu_O$ is shown in Fig. 6. Each circle represents the energy of a surface structure and the lowest energy values are interlinked by the solid lines. As can be seen, the decrease of μ_O favors the formation of oxygen vacancies but hinders zinc vacancy formation. At a certain μ_O there is

a certain favorable defect concentration, corresponding to the lowest surface energy. A particular concentration is θ=0.25, which, according to the electron-counting rule[3], makes the defective surface charge neutral and hence relatively favorable over a wide range of μ_O. This is consistent with the pronounced curvature of the solid lines at θ=0.25. It's interesting to note that the lowest energy values for oxygen vacancies agree closely with available reported data,[4] such as those for concentration θ=0.25 and 0.5 monolayer, although an orthorhombic supercell with 12 surface atoms was used here and a hexagonal supercell with 16 surface atoms was used in the previous work.

4 Summary

In summary we have for the first time calculated the surface energies of the polar surfaces for both wurtzite and zinc blende ZnO. By using a wurtzite/zinc-blend heterojunction model we can estimate the surface energies of (0001)-Zn and $(000\bar{1})$-O within a high degree of accuracy. It is found that the oxygen-terminated polar surfaces are more stable than the zinc-terminated ones within the oxygen-rich conditions, which is consistent with the experimentally observed high activity of zinc-terminated surfaces. The effects of oxygen and zinc vacancies on the surface energies are found to be strongly dependent on oxygen chemical potential μ_O. High μ_O favors zinc-deficient stoichiometry on (0001)-Zn surface and low μ_O favors oxygen-deficient stoichiometry on $(000\bar{1})$-O surface. These results shed insights on the modification of ZnO surface properties and would be useful for designing highly active ZnO nanoparticles for catalytic applications.

5 Acknowledgements

The authors acknowledge NCI National Facility for computational support of project code q27.

References

1 A. Wander, F. Schedin, P. Steadman, A. Norris, R. McGrath, T. Turner, G. Thornton and N. Harrison, *Physical Review Letters*, 2001, **86**, 3811–3814.
2 O. Dulub, U. Diebold and G. Kresse, *Physical Review Letters*, 2003, **90**, 016102.
3 M.-H. Du, S. B. Zhang, J. E. Northrup and S. C. Erwin, *Physical Review B*, 2008, **78**, 155424.
4 R. Wahl, J. V. Lauritsen, F. Besenbacher and G. Kresse, *Physical Review B*, 2013, **87**, 085313.
5 M. Bowker, H. Houghton, K. Waugh, T. Giddings and M. Green, *Journal of Catalysis*, 1983, **84**, 252–255.
6 J. Baxter, F. Wu and E. Aydil, *Applied Physics Letters*, 2003, **83**, 3797–3799.
7 Z. Wang, X. Kong and J. Zuo, *Physical Review Letters*, 2003, **91**, 185502.
8 M. Shiojiri and C. Kaito, *Journal of Crystal Growth*, 1981, **52**, 173–177.
9 Y. Ding, Z. L. Wang, T. Sun and J. Qiu, *Applied Physics Letters*, 2007, **90**, 153510.
10 Y. M. Yu and B. G. Liu, *Phys. Rev. B*, 2008, **77**, 195327.
11 A. Navrotsky, *ChemPhysChem*, 2011, **12**, 2207.
12 G. Kresse and J. Furthmuller, *Physical Review B*, 1996, **54**, 11169–11186.
13 H. Karzel, W. Potzel, M. Kofferlein, W. Schiessl, M. Steiner, U. Hiller, G. Kalvius, D. Mitchell, T. Das, P. Blaha, K. Schwarz and M. Pasternak, *Physical Review B*, 1996, **53**, 11425–11438.
14 E. Kisi and M. Elcombe, *Acta Crystallographica Section C-Crystal Structure Communications*, 1989, **45**, 1867–1870.
15 S. Zhang and S. Wei, *Physical Review Letters*, 2004, **92**, 086102.
16 B. Meyer, *Physical Review B*, 2004, **69**, 045416.
17 P. J. Linstrom and W. G. Mallard, *NIST Chemistry WebBook (http://webbook.nist.gov), NIST Standard Reference Database No. 69*, National Institute of Standards and Technology, Gaithersburg MD, 2001.
18 A. Jenichen, C. Engler and B. Rauschenbach, *Surface Science*, 2013, **613**, 74–79.
19 P. L. Liu and Y. J. Siao, *Scripta Materialia*, 2011, **64**, 483–485.
20 B. Meyer and D. Marx, *Physical Review B*, 2003, **67**, 035403.
21 A. Navrotsky, *International Journal of Quantum Chemistry*, 2009, **109**, 2647–2657.
22 J. V. Lauritsen, S. Porsgaard, M. K. Rasmussen, M. C. R. Jensen, R. Bechstein, K. Meinander, B. S. Clausen, S. Helveg, R. Wahl, G. Kresse and F. Besenbacher, *ACS NANO*, 2011, **5**, 5987–5994.
23 V. Staemmler, K. Fink, B. Meyer, D. Marx, M. Kunat, S. Girol, U. Burghaus and C. Woll, *Physical Review Letters*, 2003, **90**, 106102.